Accepted for publication in – JOM –

Published in 2014

DOI: 10.1007/s11837-014-0914-2

Compressive properties of metal matrix syntactic foams in free and constrained compression

Imre Norbert ORBULOV[a,b,c]*, Kornél MÁJLINGER[a,d]

[a]Department of Materials Science and Engineering, Faculty of Mechanical Engineering, Budapest University of Technology and Economics, Bertalan Lajos utca 7., Budapest, Hungary, 1111

[b]MTA–BME Research Group for Composite Science and Technology, Műegyetem rakpart 3., Budapest, Hungary, 1111

[c]orbulov@eik.bme.hu

[d]vmkornel@eik.bme.hu

*Corresponding author

Address: Department of Materials Science and Engineering, Faculty of Mechanical Engineering, Budapest University of Technology and Economics, Bertalan Lajos utca 7., Budapest, Hungary, 1111

Tel: +36 1 463 2386

Fax: +36 1 463 1366

E-mail: orbulov@eik.bme.hu, orbulov@gmail.com

Abstract

Metal matrix syntactic foam (MMSF) blocks were produced by inert gas assisted pressure infiltration technique. MMSFs are advanced hollow sphere reinforced composite materials having promising application fields in aviation, transport and automotive industry as well as in civil engineering. The produced blocks were investigated in free and constrained compression mode and besides the characteristic mechanical properties their deformation mechanisms and failure modes were studied. In the tests the chemical composition of the matrix material, the size of the reinforcing ceramic hollow spheres, the applied heat treatment and the compression mode were considered as investigation parameters. The monitored mechanical properties were the compressive strength, the fracture strain, the structural stiffness, the fracture energy and the overall absorbed energy. These characterising properties were strongly influenced by the test parameters. By the proper selection of the matrix and the reinforcement and by proper design, the mechanical properties of the MMSFs can be effectively tailored for specific and given applications.

Keywords

Metallic foam, compressive strength, fracture strain, structural stiffness, absorbed energy, metal matrix composite

1. Introduction

In general point of view metal matrix syntactic foams (MMSFs) are advanced metal matrix composites (MMCs), built up from thousands of ceramic or/and metallic hollow spheres (or microballoons) and a metallic matrix. Due to the particle like hollow spheres they can be considered metallic foams as well as particle reinforced MMCs. The most common matrix materials are aluminium alloys (however iron matrix syntactic foams were also reported in [1-3], while the ceramic hollow spheres are composition of various oxide ceramics (mainly Al_2O_3 and/or SiO_2). MMSFs have some significant properties such as low weight, outstanding specific mechanical properties, high mechanical energy absorption capability and good creep resistance (in case of ceramic reinforcement). It is worth to mention that the specific mechanical properties of MMSFs can be 50-100% higher than the 'conventional' foams' [4-5]. Considering these beneficial properties, MMSFs can be used as collision dampers, as material of hulls or as sound absorbers.

The most important properties of the foams are the compressive strength and the absorbed energy; therefore these properties have been widely studied. For example the quasi-static and high strain rate properties of Al- Al_2O_3 MMSFs were monitored and predicted considering the strength of the matrix material and the size of the reinforcing hollow spheres [6-8]. The effect of the hollow spheres' size on the compressive strength was also investigated. MMSFs with smaller spheres showed higher compressive strength because the spheres with smaller average diameter and wall thickness contain fewer flaws in their microstructure, than the larger ones [9, 10]. The effect of the hollow spheres' size was also investigated in the infiltration point of view. The measurements showed that the spheres with larger average diameter can be infiltrated by lower pressure that needs less investment [11, 12]. Besides conventional, uniaxial compression tests measurements were also performed in

radially constrained condition. In such cases the energy absorption capacity was extremely high in comparison with values that are typical of metal foams. These results confirmed that the MMSFs may be attractive for applications requiring a high resistance to local intrusions, in combination with low density and high compressive strength [13]. Regarding the load transfer between the reinforcing hollow spheres and the matrix, special step-by-step compression tests complemented with X-ray and/or neutron diffraction tests after each step were performed. The analysis showed that the hollow spheres have at least the same importance in the MMSFs as the matrix material itself. The fracture strength of the spheres and the yield strength of the matrix together determine the failure stress of the MMSFs [14, 15]. Hybrid MMSFs with two, different diameter, but same materials hollow spheres and with Al matrix was also investigated in uniaxial and in constrained compression. In the latter case all MMSFs failed by the progressive collapse of the ceramic microspheres, while in free compression the MMSFs failed by brittle rupture [16-18]. High strain rate compressive tests again proved that the smaller microballoons with thinner wall are more beneficial due to their higher compressive strength, more flawless microstructure and better mechanical stability [19]. MMSFs produced by the combination of hollow steel spheres and aluminium alloy matrix were developed and their characterizing investigations showed superior compressive strength and energy absorption capacity [20-22]. In a series of comprehensive works microballoons in the range of 30–50 vol% were used to produce aluminium matrix syntactic foams by stir-casting technique. The synthesised MMSF was characterised in terms of microstructures, hardness and compressive deformation behaviour at elevated temperatures and at high strain rate too. All of the measurements confirmed considerably higher mechanical properties than those of conventional aluminium foams [23-27].

Moreover results were published about the long term creep [28], wear and corrosive properties [24, 29-31] properties and global, depth sensing, dynamic and local hardness [30, 32] of MMSFs. Nowadays, the wear mechanism of MMSFs is also popular research field, because the ceramic hollow spheres can act as lubricant reservoirs and this can cause significant improvement in wear properties. In summary, in the works mentioned above the results of quasi-static, dynamic, free and constrained compression test were published in details and many parameters (like hollow spheres' grade and size, porosity, type of matrix material etc.) were taken into account.

Beside this, papers on the problems of MMSF production were also published [33-37]. Generally, the results of existing infiltration models give satisfactory predictions on the infiltrated length as the function of infiltration parameters (pressure, time and temperature) in the case of simple systems, however large deviations from the predicted results can be observed in case of reactive systems having complex geometry, changing permeability and short infiltration times.

A few papers were published on the determination of the elastic properties of syntactic foams and sandwich structures consisting syntactic foams [38, 39, 40]. These articles are based on a three phase unit cell model considering the matrix – wall – porosity structure of the syntactic foams. Subsequent studies took into account the influence of weak interface between the inclusion (hollow spheres) and the matrix material [41]; and presented numerical studies to predict the elastic properties of the foams [42]. Analytical functions to describe the typical stress – strain curves of the MMSFs were also presented [43].

Considering the above mentioned works the aim of this paper is to examine the effect of the chemical composition of the matrix material, the size of the reinforcing ceramic hollow spheres, the

applied heat treatment and especially the compression mode (free or constrained) on the mechanical properties and failure mechanisms of MMSFs.

2. Materials and experimental methods

The investigated materials were self-made MMSFs, produced by inert gas assisted low pressure infiltration technique in a special furnace (Fig. 1). The hollow spheres were poured into a 360 mm high carbon steel mould (cross-section: 80 × 80 mm) to the half and they were densified by gentle tapping to get randomly closed pack structure (RCPS, corresponding to 64 vol% reinforcement fraction [44]). Subsequently, a layer of alumina separator and a solid block of matrix material was placed on the top of the hollow spheres. The prepared mould was situated into the infiltration chamber, the chamber was closed and the whole system was evacuated by a vacuum pump (rough vacuum). The system was heated by three heating zones and the temperatures of the matrix block and the hollow spheres were continuously monitored by two thermocouples. After the melting of the matrix the molten metal sealed the mould above the separator layer. The vacuum pump was switched off and argon gas was let into the chamber. Due to this a pressure difference was built up in the mould (vacuum under the molten metal, argon pressure above it). This pressure difference infiltrated the metal into the space between the hollow spheres. After solidification the mould was removed from the chamber and water cooled to room temperature. Then the complete MMSF block (80 × 80 × 180 mm) could be removed from the mould. For further details about the production process please refer to [37, 45].

Basically four MMSF blocks were produced by the combination of four matrix alloys (Al99.5, AlSi12, AlMgSi1 and AlCu5, see Table 1 for chemical composition) and Globocer grade ceramic hollow spheres (supplied by Hollomet GmbH [46], designated as G). The blocks were solution treated (O) and in the case of AlMgSi1 and AlCu5 matrix precipitation hardened (T6). The parameters of heat treatments are listed in Table 2. Moreover, in order to investigate the size effect of the reinforcement, two more, namely Al99.5 and AlSi12 matrix MMSF blocks were produced by E-Sphere reinforcement (supplied by Envirospheres Ltd. [47], designated as S). The chemical composition of the ceramic hollow spheres were the same, as well as their wall thickness to diameter ratio were similar. The main difference between them was in their average outer diameter: the Globocer's diameter is larger than E-Spheres' by one magnitude. The detailed properties are listed in Table 3.

The MMSF blocks and specimens were designated according to their constituents and heat treatment. For example Al99.5-G-O stands for a specimen with Al99.5 matrix reinforced by Globocer grade ceramic hollow spheres and in solution treated state.

Cylindrical specimens for free and constrained compression tests were machined from the blocks. The diameter and the height of the specimens were 10 mm and 15 mm respectively (the aspect ratio was 1.5). Two typical optical microscope images are shown in Fig. 2. In order to get average results five specimens were compressed for each MMSF block and condition. It means in summary 80 compression tests (4 matrices reinforced by G grade spheres × 2 compression mode × 5 specimens in solution treated state, 2 matrices reinforced by G grade spheres × 2 compression mode × 5 specimens in precipitation hardened state and 2 matrices reinforced by S grade spheres × 2 compression mode × 5 specimens in solution treated state). The compressive tests were carried out

on a MTS810 hydraulic universal testing machine between polished hard plates (free compression) and in a cylindrical tool steel die (constrained compression). The specimens and the tools were lubricated by anti-seize material with MoS_2 content. The deformation rate during the compression tests was maintained at 0.01 s^{-1} in order to ensure quasi static conditions.

During the tests the engineering stress – engineering strain curves were registered, processed and evaluated in order to get information about the mechanical properties of MMSFs in free and constrained compression.

3. Results and Discussion

3.1 Stress – strain curves

The registered engineering stress – engineering deformation curves have typical forms. As representative examples, in Fig.3a and in Fig. 3b the registered curve of an Al99.5-S-O sample in the case of free and constrained compression are plotted respectively. The stress – strain curves of free compression (Fig. 3a) can be divided into three main parts containing overall five sections as explained and published in previous papers [44, 48]. These curves have five main characterising parameters. The slope of the initial part is defined as structural stiffness (S (MPa), see [49] about the standardised compression tests of cellular materials). At point B the recorded curve deviates from the initial linear part, indicating plastic deformation. At the end of the initial part – at point C – a local maximum occurs in the diagram, the stress reaches the compressive strength (σ_C (MPa)) at the fracture strain (ε_C (%)) [49]. At this point the first crack appears in the specimen and a large and sudden drop in the stress value can be observed due to the reduced load bearing capacity caused by the fracture of the hollow spheres and the movement of the recently formed specimen halves. From point D to E the fracture band expanded, the crack became thicker and the neighbouring hollow spheres broke. This deformation phenomenon consumed significant strain and mechanical energy due to the fracture of the ceramic hollow spheres and due to the plastic deformation of the matrix. The area up to the fracture strain and up to the end of the test (loading) are the fracture energy (W_C (Jm^{-3})) and the overall absorbed energy (W_L (Jm^{-3})) respectively. The absorbed energies are important characterising parameters of the MMSFs in compression, as they indicate the damping and protecting capability of the MMSFs against a blast, collision or simple vibration. The trend of the plateau region can be ascending or constant (usually ascending because the densifying material needs higher force to be deformed) and it may contain larger drops or local maximums due to secondary cracks. In the case of constrained compression, the stress – strain curves (Fig. 3b) run similar up to point C and the structural stiffness, the compressive strength, the fracture strain and the fracture energy can be identified. After the appearance of the first crack the stress drop is significantly smaller between points C and D, due to the constrained movement of the specimen. From point D the stress increases continuously up to point E. The breakage of the hollow spheres and the deformation of the matrix material require higher and higher force, because the specimen can only deform vertically. The matrix material can occupy the freed space due to the breakage of the ceramic hollow spheres; however this needs significant stress levels. The process was stopped at 1000 MPa (point E) due to the load bearing capacity of the testing machine and tool. If the test could be continued the stress would increase faster and faster, the strain at which the stress reach ‘infinite’ (in engineering point of view, let’s say 10000 MPa) is called densification limit (ε_D (%)). After point E

the specimen should be unloaded, because it is still intact. The unloading process recovers elastic mechanical energy (W_{UL} (Jm^{-3})), that is also a characteristic property.

In summary the structural stiffness, the compressive strength, the fracture and densification strains and the different absorbed and recovered mechanical energy values can be used to characterize the compressive behaviour of the MMSFs.

3.2 Characterising properties

The properties mentioned in the previous section were monitored according to the compression modes, hollow sphere sizes, heat treatments and the chemical composition of the matrix materials. First, the compressive strength values are plotted in Fig. 4. On the first four pair of bars the effect of the chemical composition can be observed in solution treated state. As it was expected the technical purity aluminium (Al99.5) MMSF specimens had the lowest compressive strength. As the amount of alloying increased, the compressive strength increased accordingly. In the case of lower alloying (Al99.5 and AlMgSi1) the difference between the free and constrained compression were larger, in constrained compression the compressive strength were higher. In the case of higher alloying (AlSi12 and AlCu5) the difference between the free and constrained compression became negligible and remained in between the scatters. In the case of T6 treated condition the compressive strength increased significantly (~50% and ~40% in the case of AlMgSi1 and AlCu5 respectively). However with this increment the MMSFs became more brittle and therefore the scatters became higher. Generally, the heat treated specimens in constrained compression showed higher compressive strength, but the values remained between the (widened) scatter bars. The smaller hollow spheres ensured higher compressive strength because the smaller diameter and higher curvature gave higher compressive strength and mechanical stability to them. Moreover, smaller wall thickness ensures lower probability for deflections; therefore the small, S grade hollow spheres had higher compressive strength than the larger, G grade hollow spheres with thicker walls and more defects. In the case of smaller hollow spheres the compression mode and the chemical composition of the matrix had no significant influence on the compressive strength.

Fig. 5 shows the measured fracture strain values. Every alloying had the same effect in the case of G grade reinforced cases, namely caused ~20% drop in the fracture strain, due to the matrix became more rigid. The T6 heat treatment caused minimal increment in the fracture strain due to the higher load bearing capacity of the matrix alloy. In the case of solution treated state the compression mode had insignificant effect on the fracture strains, while in T6 treated condition the fracture strain was slightly higher in the constrained mode. This indicates that, in T6 condition the matrix material was more sensitive to the multi-axial stress state, than in solution treated state. The smaller, S grade ceramic hollow spheres ensured almost twice as much higher fracture strains in free compression mode than G grade hollow spheres. In constrained compression mode the fracture strain became smaller, showing that the smaller hollow spheres with thinner wall are more sensitive to multi-axial stress state, than the larger, G grade hollow spheres with significantly thicker wall (but almost the same wall thickness to diameter ratio).

The structural stiffness values are plotted in Fig. 6. The structural stiffness altered similarly to the compressive strength in the case of free compression and G grade hollow sphere reinforcement. Moreover the stiffness was strongly influenced by the matrix material: the soft, Al99.5 MMSFs had the lowest structural stiffness, while the stiffness was increased ~50% by low alloying and ~100% by

strong alloying regardless to the compression mode. In the compression mode point of view the constrained compression conditions resulted in lower structural stiffness, because in multi-axial stress state the plastic deformation of the matrix could occur earlier and therefore the stiffness was apparently lower. In the case of T6 heat treatment the structural stiffness proved to be higher, due to the higher strength of the MMSFs. The increment was ~40% and ~10% in the case of AlMgSi1 and AlCu5 matrix respectively. In the case of smaller hollow spheres the situation was reversed and the stiffness was mainly determined by the ceramic hollow spheres, not by the matrix material: the values were similar regardless to the matrix material. Moreover the stiffness was higher in the case of constrained compression that proves the same: the smaller spheres showed lower fracture strain (Fig. 5), due to their sensitivity to multi-axial stress state and this phenomenon strongly decreased the structural stiffness.

The densification limits characterise the constrained compression specimens only, the values are plotted in Fig. 7. As it can be observed in Fig. 7, the density limit is definitely a structure dependent property and therefore it is influenced only by the size and the distribution of the applied ceramic hollow spheres (besides the original density of the MMSFs that is similar in all of our cases).

Besides the above mentioned mechanical properties the mechanical absorbing capabilities have important role on the application of MMSFs as vibration or collision dampers. The energy absorbed to the appearance of the first, initial crack in the specimen is called fracture energy (Fig. 8). In solution treated state the fracture energy of the specimens depended mainly on the ceramic hollow sphere size. In the case of G grade reinforcement the matrix had almost no effect on the fracture strain, only the T6 heat treatment increased the level of fracture strain ~70%, due to the significantly stronger matrix material. Similarly, the different compression modes resulted in almost the same fracture strain values (within scatters). In the case of S grade reinforcement the same trends can be observed. The fracture energies were significantly (about 2.5 times) higher and the matrix materials had negligible effect on them. However the compression mode strongly influenced the fracture energy: in constrained mode the energies were lower, again confirming the strong sensitivity of smaller spheres (with thinner wall) to multi-axial stress state.

The overall absorbed mechanical energies are plotted in Fig. 9. In free compression mode the absorbed mechanical energy was influenced mainly by the composition of the matrix material. The stronger matrix ensured higher plateau (the curve between point D and E in Fig. 3a) stress levels and that resulted in higher absorbed energies. This was not really affected by the T6 heat treatments, because at higher stress levels more cracks can occur in the whole specimens with small stress relaxations and therefore the overall energy absorbtion was not significantly changed. In free compression the smaller hollow spheres performed better and due to their higher strength ensured ~65% and 20% higher energy absorbtion in the case of Al99.5 and AlSi12 matrix, respectively. During constrained compression tests the overall absorbed energies proved to be much higher (at least 2.5 times higher), than in free compression because of the higher required force to deform the specimens in multi-axial stress state. The level of the absorbed energy was mainly influenced by the size of the hollow spheres. In this mode the plastically deforming matrix material had to be pushed into the small spaces were the hollow spheres were broken and this needed significantly higher stresses than in the case of larger hollow spheres (and larger available spaces after their breakage), where the plastic deformation is less retarded.

Finally the recovered energies in the case of constrained compression mode are plotted in Fig. 10. The recovered energies were mainly influenced by the heat treatment and hollow sphere size. The T6 treatment decreased the recoverable energy significantly, because the stronger matrix material resulted in smaller overall deformation at a given load level, and due to this the elastic part of the deformation also became smaller. Besides this, the recoverable energies were independent in the matrix material and hollow sphere size point of view.

3.3 Failure modes

The failure mode of the investigated MMSFs differed a lot, depending on the compression mode and on the ceramic hollow sphere size. In Fig. 11 the free compression is highlighted. The G and S grade hollow sphere reinforcements resulted distinct failure modes. In the case of G grade reinforcement the specimens showed extensive barrelling (Fig. 11a). Two deformation cones were formed at the top and at the bottom of the specimens. The largest deformation was occurred between these cones. The side of the specimens also deformed and began to detach due to excessive barrelling. The whole process absorbed lot of mechanical energy, due to the deformation of the matrix and breakage of the hollow spheres. In the case of S grade reinforcement the deformation was ruled by the formation of a definite shear crack, along ~45° to the vertical loading direction (Fig. 11b). The crack divided the specimen into two halves and the halves slid on each other, thickening the damaged zone and absorbing high amount of mechanical energy. It is worth to emphasize that, the other parts of the specimen remained unharmed and could absorb more energy.

The failure modes in constrained compression are shown in Fig. 12. Both in the cases of G and S grade hollow spheres the failure mode was the same. Under vertical loading the hollow spheres were crashed and compressed (Fig. 12a, 12b and inset magnification 12c). As it can be observed, all the hollow spheres were broken and the whole specimen was damaged, however until this condition the specimen absorbed at least 2 to 4 times higher energy than in free compression. This property makes MMSFs exceptional collision dampers in case of constrained conditions (for example in the case of hollow structures filled by MMSF).

4. Conclusions

From the above detailed measurements and investigations the following concluding remarks can be drawn.

- MMSFs in free and constrained compression have typical, but very different stress – strain diagrams. Important characterising properties can be determined from both diagram type, like compressive strength, fracture strain, structural stiffness, fracture energy, absorbed mechanical energy (for both compression modes), densification limit and recovered energy (for constrained compression mode).

- The compressive strength, fracture strain and structural stiffness were strongly influenced by the composition of the matrix material, the grade of the reinforcement, the heat treatment and the compression mode. By proper selection of the mentioned conditions the properties of the MMSFs can be tailored for specific given applications.

- The densification limit in the case of constrained compression was mainly influenced by the hollow spheres' size.
- In the case of G grade reinforcement the fracture energies was mainly influenced by the T6 heat treatment. In the case of S grade hollow spheres the compression mode was decisive, and in constrained condition the S grade hollow spheres showed emphasized sensitivity to multi-axial loading.
- Generally, the overall absorbed mechanical energy was strongly influenced by the compression mode. In constrained compression the absorbed energies were at least 2.5 times higher than in free compression.
- The amount of recoverable energy in the case of constrained compression was mainly influenced by the applied heat treatment.
- The failure of the specimens in free and in constrained compression showed distinct modes. In free compression barrelling or shearing can be isolated according to G or S grade reinforcement respectively. In constrained compression all of the hollow spheres in the specimens were crashed in the direction of the loading and the specimens suffered severe plastic deformation axially.

Acknowledgements

This research was supported by the European Union and the State of Hungary, co-financed by the European Social Fund in the framework of TÁMOP 4.2.4. A/2-11-1-2012-0001 'National Excellence Program'.

References

[1] Peroni L, Scapin M, Avalle M, Weise J, Lehmhus D. Dynamic mechanical behavior of syntactic iron foams with glass microspheres. Mater Sci Eng A 2012;552:364-75.
[2] Peroni L, Scapin M, Avalle M, Weise J, Lehmhus D, Baumeister J, et al. Syntactic Iron Foams - On Deformation Mechanisms and Strain-Rate Dependence of Compressive Properties. Adv Eng Mater 2012;14:909-18.
[3] Weise J, Lehmhus D, Baumeister J, Kun R, Bayoumi M, Busse M. Production and Properties of 316L Stainless Steel Cellular Materials and Syntactic Foams. Steel Res Int 2013 doi:10.1002/srin.201300131 (in press)
[4] Babcsán N, Leitlmeier D, Banhart J. Metal foams—high temperature colloids: Part I. Ex situ analysis of metal foams. Colloid Surf A: Physicochem Eng Asp 2005;261:123-30.
[5] Babcsán N, Moreno FG, Banhart J. Metal foams—High temperature colloids: Part II: In situ analysis of metal foams. Colloid Surf A: Physicochem Eng Asp 2007;309:254-63.
[6] Santa Maria JA, Schultz BF, Ferguson JB, Rohatgi PK. Al–Al_2O_3 syntactic foams – Part I: Effect of matrix strength and hollow sphere size on the quasi-static properties of Al-A206/Al_2O_3 syntactic foams. Mater Sci Eng A 2013;582:415-22.
[7] Ferguson JB, Santa Maria JA, Schultz BF, Rohatgi PK. Al–Al_2O_3 syntactic foams—Part II: Predicting mechanical properties of metal matrix syntactic foams reinforced with ceramic spheres. Mater Sci Eng A 2013;582:423-32.
[8] Santa Maria JA, Schultz BF, Ferguson JB, Guptan N, Rohatgi PK. Effect of hollow sphere size and size distribution on the quasi-static and high strain rate compressive properties of Al-A380-Al_2O_3 syntactic foams. J Mater Sci 2013 doi:10.1007/s10853-013-7810-y (in press)
[9] Wu GH, Dou ZY, Sun DL, Jiang LT, Ding BS, He BF. Compression behaviors of cenosphere–pure aluminum syntactic foams. Scripta Mater 2007;56:221-4.
[10] Palmer RA, Gao K, Doan TM, Green L, Cavallaro G. Pressure infiltrated syntactic foams—Process development and mechanical properties. Mater Sci Eng A 2007;464:85-92.
[11] Rohatgi PK, Kim JK, Gupta N, Alaraj S, Daoud A. Compressive characteristics of A356/fly ash cenosphere composites synthesized by pressure infiltration technique. Compos Part A 2006;37:430-7.
[12] Rohatgi PK, Gupta N, Schultz BF, Luong DD. The synthesis, compressive properties, and applications of metal matrix syntactic foams. JOM 2011;63:36-42.
[13] Kiser M, He MY, Zok FW. The mechanical response of ceramic microballoon reinforced aluminum matrix composites under compressive loading. Acta Mater 1999;47:2685-94.
[14] Balch DK, O'Dwyer JG, Davis GR, Cady CM, Gray Iii GT, Dunand DC. Plasticity and damage in aluminum syntactic foams deformed under dynamic and quasi-static conditions. Mater Sci Eng A 2005;391:408-17.
[15] Balch DK, Dunand DC. Load partitioning in aluminum syntactic foams containing ceramic microspheres. Acta Mater 2006;54:1501-11.
[16] Tao XF, Zhang LP, Zhao YY. Al matrix syntactic foam fabricated with bimodal ceramic microspheres. Mater Des 2009;30:2732-6.
[17] Tao XF, Zhao YY. Compressive behavior of Al matrix syntactic foams toughened with Al particles. Scripta Mater 2009;61:461-4.
[18] Tao XF, Zhao YY. Compressive failure of Al alloy matrix syntactic foams manufactured by melt infiltration. Mater Sci Eng A 2012;549:228-32.
[19] Dou ZY, Jiang LT, Wu GH, Zhang Q, Xiu ZY, Chen GQ. High strain rate compression of cenosphere-pure aluminum syntactic foams. Scripta Mater 2007;57:945-8.
[20] Rabiei A, O'Neill AT. A study on processing of a composite metal foam via casting. Mater Sci Eng A 2005;404:159-64.
[21] Vendra LJ, Rabiei A. A study on aluminum–steel composite metal foam processed by casting. Mater Sci Eng A 2007;465:59-67.

[22] Rabiei A, Garcia-Avila M. Effect of various parameters on properties of composite steel foams under variety of loading rates. Mater Sci Eng A 2013;564:539-47.
[23] Mondal DP, Das S, Ramakrishnan N, Uday Bhasker K. Cenosphere filled aluminum syntactic foam made through stir-casting technique. Compos Part A 2009;40:279-88.
[24] Mondal DP, Das S, Jha N. Dry sliding wear behaviour of aluminum syntactic foam. Mater Des 2009;30:2563-8.
[25] Mondal DP, Jha N, Badkul A, Das S, Khedle R. High temperature compressive deformation behaviour of aluminum syntactic foam. Mater Sci Eng A 2012;534:521-9.
[26] Mondal DP, Jha N, Gull B, Das S, Badkul A. Microarchitecture and compressive deformation behaviour of Al-alloy (LM13)–cenosphere hybrid Al-foam prepared using $CaCO_3$ as foaming agent. Mater Sci Eng A 2013;560:601-10.
[27] Mondal DP, Goel MD, Das S. Effect of strain rate and relative density on compressive deformation behaviour of closed cell aluminum–fly ash composite foam. Mater Des 2009;30:1268-74.
[28] Couteau O, Dunand DC. Creep of aluminum syntactic foams. Mater Sci Eng A 2008;488:573-9.
[29] Ramachandra M, Radhakrishna K. Effect of reinforcement of flyash on sliding wear, slurry erosive wear and corrosive behavior of aluminium matrix composite. Wear 2007;262:1450-62.
[30] Ramachandra M, Radhakrishna K. Synthesis-microstructure-mechanical properties-wear and corrosion behavior of an Al-Si (12%)-Flyash metal matrix composite. J Mater Sci 2005;40:5989-97.
[31] Rohatgi PK, Guo RQ. Mechanism of abrasive wear of Al-Si hypoeutectic alloy containing 5 vol% fly ash. Tribol Lett 1997;3:339-47.
[32] Orbulov I, Németh Á. Global, depth sensing and dynamic hardness of metal matrix syntactic foams. Per Pol Mech Eng 2009;53:93-9.
[33] Bárczy T, Kaptay G. Modeling the infiltration of liquid metals into porous ceramics. Mater Sci Forum. 2005;473-474:297-302.
[34] Trumble KP. Spontaneous infiltration of non-cylindrical porosity: Close-packed spheres. Acta Mater 1998;46:2363-7.
[35] Rohatgi PK, Guo RQ, Iksan H, Borchelt EJ, Asthana R. Pressure infiltration technique for synthesis of aluminum–fly ash particulate composite. Mater Sci Eng A 1998;244:22-30.
[36] Orbulov IN. Metal matrix syntactic foams produced by pressure infiltration—The effect of infiltration parameters. Mater Sci Eng A 2013;583:11-9.
[37] Orbulov IN, Dobránszky J. Producing metal matrix syntactic foams by pressure infiltration. Per Pol Mech Eng 2008;52:35-42.
[38] Bardella L, Genna F. Elastic design of syntactic foamed sandwiches obtained by filling of three-dimensional sandwich-fabric panels. Int J Sol Struct 2001;38:307-33.
[39] Bardella L, Genna F. On the elastic behavior of syntactic foams. Int J Sol Struct 2001;38:7235-60.
[40] Marur PR. Effective elastic moduli of syntactic foams. Mater Lett 2005;59:1954-7.
[41] Marur PR. Influence of imperfect interface on the elastic moduli of syntactic foams. Computat Mater Sci 2009;46:327-32.
[42] Marur PR. Numerical estimation of effective elastic moduli of syntactic foams. Finite Elements in Analysis and Design 2010;46:1001-7.
[43] Orbulov IN, Májlinger K. Description of the compressive response of metal matrix syntactic foams. Mater Des 2013;49:1-9.
[44] Jaeger HM, Nagel SR. Physics of the Granular State. Science. 1992;5051:1523-31.
[45] Orbulov IN, Ginsztler J. Compressive characteristics of metal matrix syntactic foams. Compos Part A 2012;43:553-61.
[46] Hollomet GmbH <http://www.hollomet.com/home.html> [accessed: 20.11.13].
[47] Envirospheres Ltd. <http://www.envirospheres.com/products.asp> [accessed: 20.11.13].
[48] Orbulov IN. Compressive properties of aluminium matrix syntactic foams. Mater Sci Eng A 2012;555:52-6.
[49] Testing of metallic materials – Compression test of metallic cellular materials DIN 50134 standard; October 2008

Table captions

Table 1. Chemical composition of the applied matrix materials (only the significant elements are tabulated)

Matrix	Main components (wt%)				Closest ASM equivalent
	Al	Si	Mg	Cu	
Al99.5	99.5	-	-	-	Al1050
AlSi12	86	12	-	-	A413
AlMgSi1	97	1	1.2	0.3	Al6061
AlCu5	95	-	-	4.5	Al2011

Table 2. Parameters of the applied heat treatments

Matrix	Solution treatment		Cooling medium	Precipitation hardening		Cooling medium
	Temperature, T (°C)	Time, t (h)		Temperature, T (°C)	Time, t (h)	
Al99.5	500	1	water	-	-	-
AlSi12	500	1	water	-	-	-
AlMgSi1	520	1	water	170	14	water
AlCu5	500	1	water	160	14	water

Table 3. Morphological properties and phase constitution of the ceramic hollow spheres [37, 46, 47]

Type	D (µm)	ρ (gcm^{-3})	η (-)	Main components (wt%)		
				Al_2O_3	Amorphous SiO_2	Mullite
S	150	0.691	0.0437	30-35	45-50	19
G	1450	0.816	0.0414			

D: average diameter

ρ: bulk density at 64 vol%

η: average wall thickness to diameter ratio

Figure captions

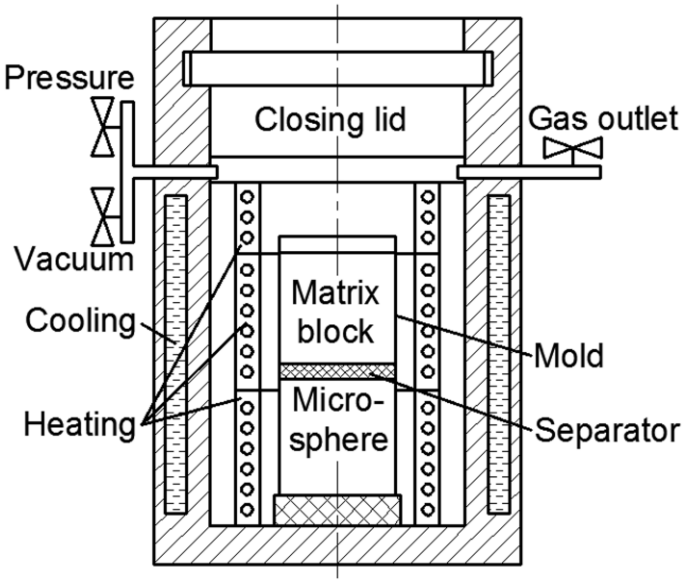

Fig. 1. Schematic sketch of the infiltration chamber

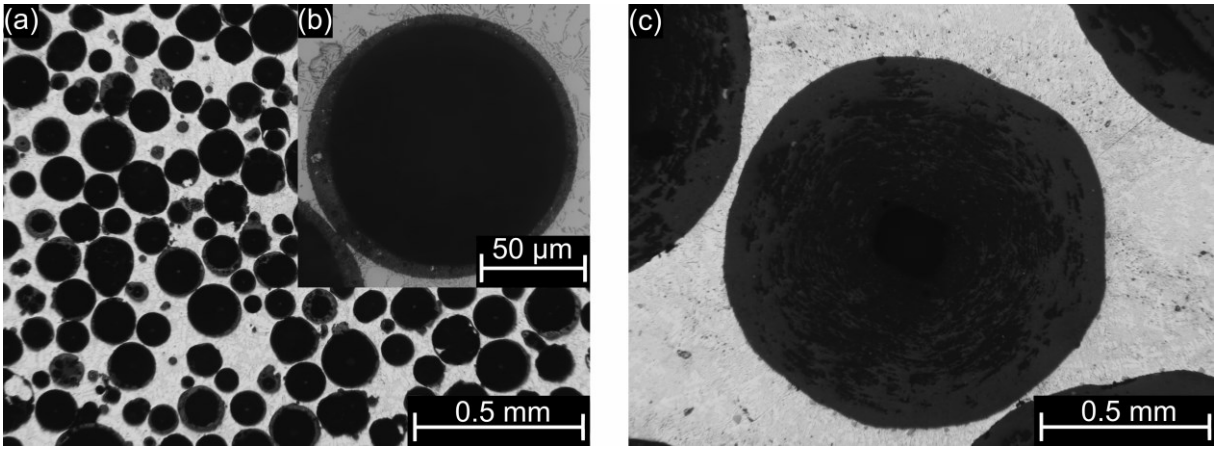

Fig. 2. Typical optical microscope images of AlSi12-S-O (a) and Al99.5-G-O type MMSFs

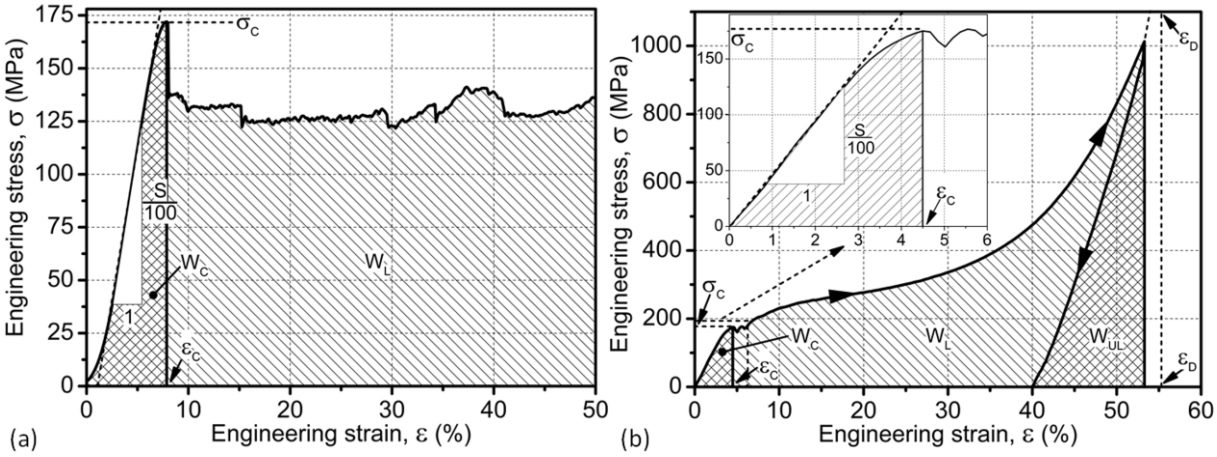

Fig. 3. Representative engineering stress – strain curves of Al99.5-S-O samples in free (a) and in constrained (b) compression

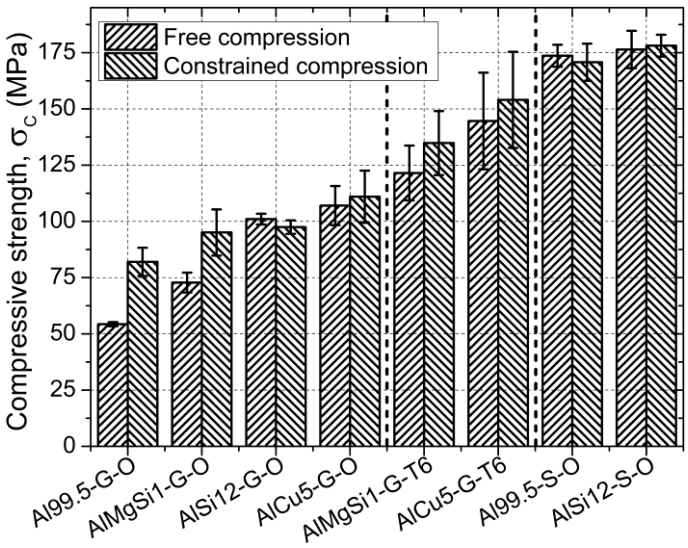

Fig. 4. The compressive strengths of the investigated MMSFs

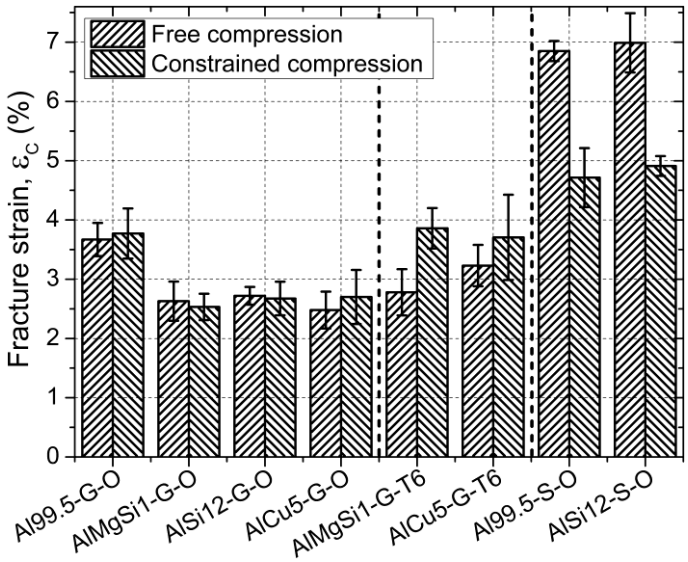

Fig. 5. The fracture strains of the investigated MMSFs

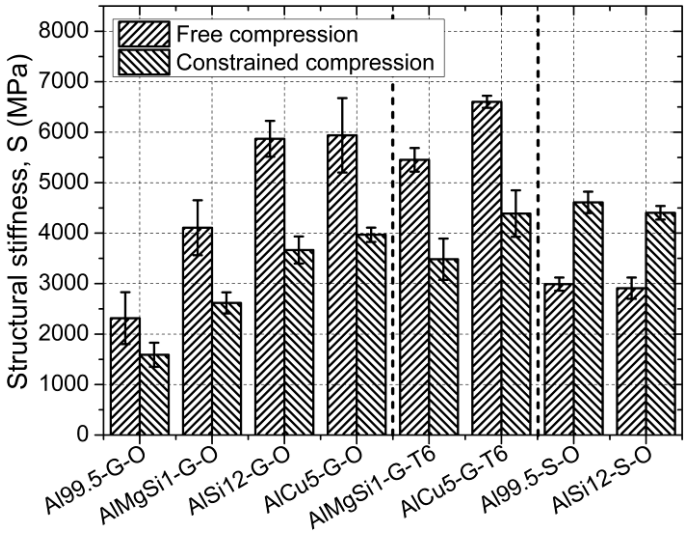

Fig. 6. The structural stiffness values of the investigated MMSFs

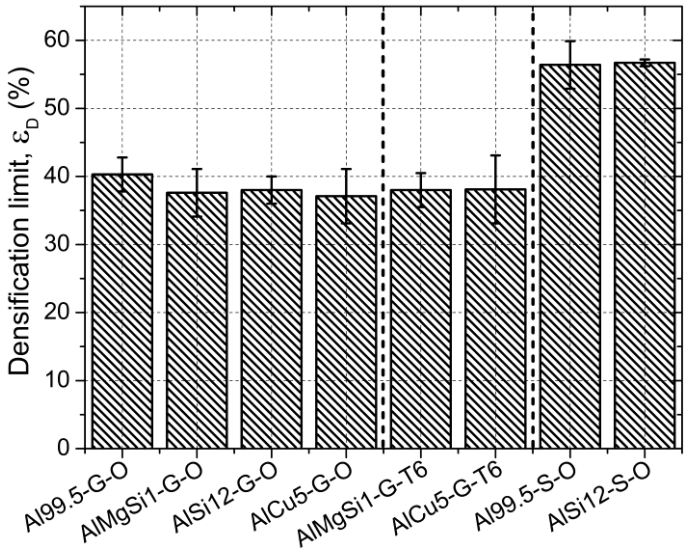

Fig. 7. The densification limits of the investigated MMSFs in constrained compression

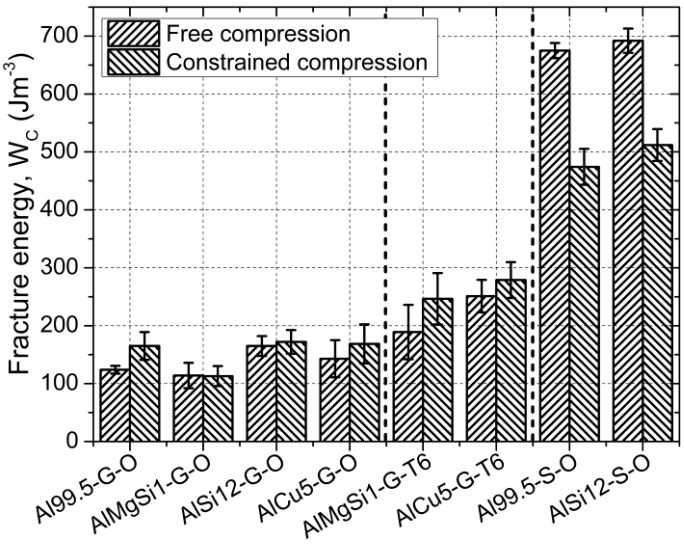

Fig. 8. The fracture energies of the investigated MMSFs

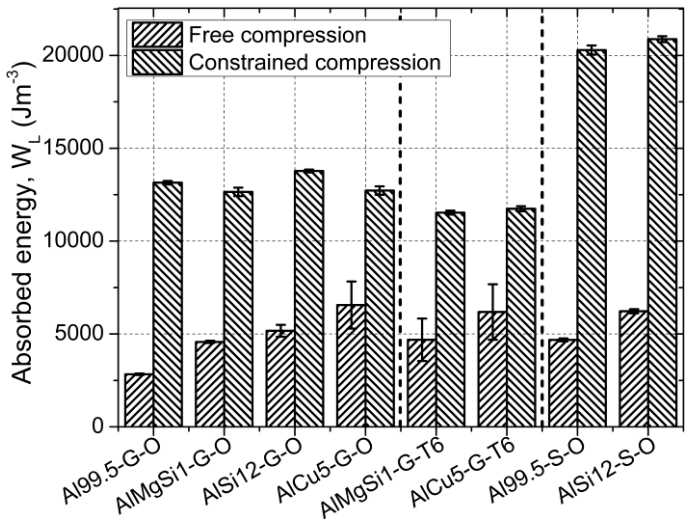

Fig. 9. The overall absorbed mechanical energies of the investigated MMSFs during uploading

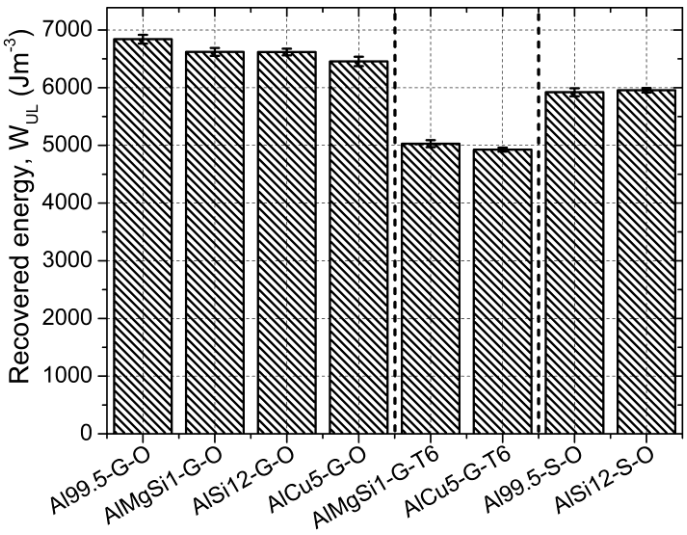

Fig. 10. The recovered energies of the investigated MMSFs during unloading in constrained compression

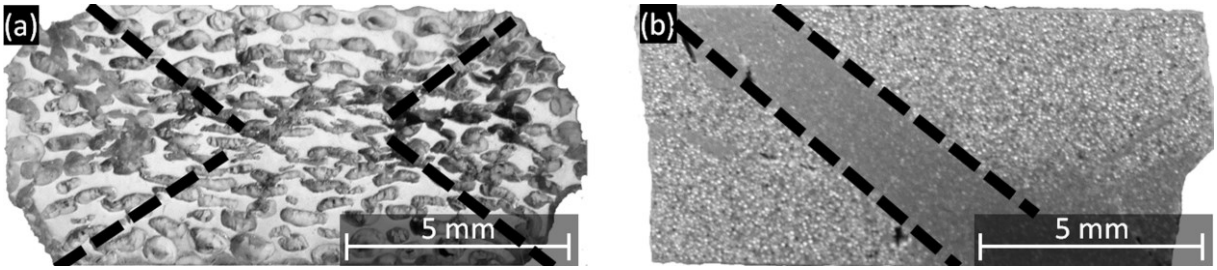

Fig. 11. Failure modes of G grade (a) and S grade (b) AlMgSi1 matrix syntactic foams in free compression

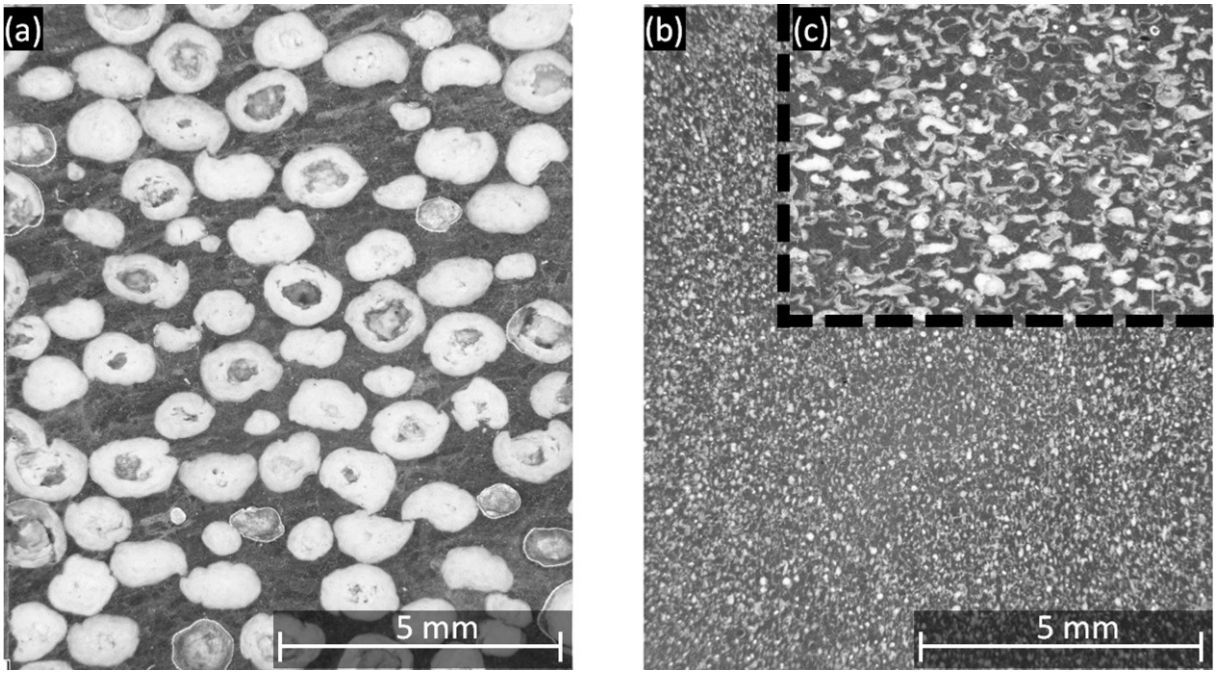

Fig. 12. Failure modes of G grade (a) and S grade (b and c) AlMgSi1 matrix syntactic foams in constrained compression